RESEARCH ARTICLE | JULY 31 2018

Acoustic Lock: Position and orientation trapping of non-spherical sub-wavelength particles in mid-air using a single-axis acoustic levitator

L. Cox ; A. Croxford; B. W. Drinkwater; A. Marzo

https://doi.org/10.1063/1.5042518

Acoustic Lock: Position and orientation trapping of non-spherical sub-wavelength particles in mid-air using a single-axis acoustic levitator

L. Cox,[a] A. Croxford, B. W. Drinkwater, and A. Marzo
Faculty of Engineering, University of Bristol, Bristol BS8 1TR, United Kingdom

(Received 1 June 2018; accepted 17 July 2018; published online 31 July 2018)

We demonstrate acoustic trapping in both position and orientation of a non-spherical particle of sub-wavelength size in mid-air. To do so, we multiplex in time a pseudo-one-dimensional vertical standing wave and a twin-trap; the vertical standing wave provides converging forces that trap in position, whereas the twin-trap applies a stabilising torque that locks the orientation. The device operates at 40 kHz, and the employed multiplexing ratio of the 2 acoustic fields is 100:50 (standing:twin) periods. This ratio can be changed to provide tunability of the relative trapping strength and converging torque. The torsional spring stiffness of the trap is measured through simulations and experiments with good agreement. Cubes from $\lambda/5.56$ (1.5 mm) to $\lambda/2.5$ (3.4 mm) side length were stably locked. We also apply this technique to lock different non-spherical particles in mid-air: cubes, pyramids, cylinders, and insects such as flies and crickets. This technique adds significant functionality to mid-air acoustic levitation and will enable applications in micro-scale manufacturing as well as containment of specimens for examination and 3D-scanning. *Published by AIP Publishing.* https://doi.org/10.1063/1.5042518

Acoustic radiation force devices are employed for trapping and manipulating particles without contamination.[6] They are becoming a fundamental tool for applications such as inspection or containerless transportation of small objects[5,8] and even the study of small animals.[21,24]

Acoustic levitation enables the robust trapping of different materials on the order of millimetre sizes. Furthermore, acoustic levitation presents various advantages compared to other methods. In optical trapping, the particles must be in the 0.01–10 μm range and either dielectric or optically transparent.[18] It is also orders of magnitude weaker than acoustic forces for the same input power.[16] Magnetic levitation can hold samples in mid-air,[7] but it is limited to ferromagnetic or diamagnetic materials.[4,9] Finally, aerodynamic levitation[26] agitates the sample and can alter its behaviour and electrostatic levitation requires complex control systems for a limited range of sample materials.[18] These restrictions do not apply to acoustic levitation.

The single-axis acoustic levitator is one of the most common methods of achieving mid-air levitation. In this levitator, two opposing emitters are used to create a standing wave that traps the particles at its nodes; however, a single-sided source and a reflector are also a common way of creating vertical standing waves.[23]

Single-axis levitators are relatively simple in design, and the high amplitude pseudo-one-dimensional standing wave[5] enables trapping of a multitude of different samples. For this reason, significant research has been conducted into improving its design[3,14] and understanding its behaviour.[2,22]

Previous work in mid-air acoustic trapping has largely been focused on spherical particles or fluid droplets.[12] However, many samples of interest are non-spherical, e.g., cuboids, spheroids, or insects. When these particles are inserted inside a single-axis levitator, they typically spin on their vertical axis.[19,22,25] This hinders observation, characterisation, or assembly of non-spherical samples.

Stable trapping of non-spherical particles has mainly been demonstrated in 2D arrangements.[20] Non-spherical particles can be controlled in orientation with an acoustic tractor beam,[16] but this is currently less useful for most practical applications since the forces are 30 times weaker than a vertical standing wave (as is used in a single-axis levitator) with the same pressure levels.

Here, we propose a technique to stop the undesirable spinning of levitated samples in a single-axis levitator and thus stably trap a non-spherical particle, in both the position and the orientation. We call this technique Acoustic Lock in reference to the Quantum Lock or Flux Pinning effect[13] which uses magnetic levitation and a superconductor to achieve the same result.

The proposed system employs a rapid switching in time between a pseudo-one-dimensional vertical standing wave[23] and a twin-trap.[16] The vertical standing wave provides a strong trapping force and thus gives vertical support against gravity and the twin-trap provides a converging torque against the natural tendency of the particle to spin. The pressure amplitudes of these two types of traps are shown in Fig. 1. Figure 1(c) shows the symmetrical pressure field of a pseudo-one-dimensional standing wave, whilst Fig. 1(d) shows a twin-trap consisting of two regions of high pressure with a low pressure region between creating acoustic tweezers holding the particle from the sides.

Previous techniques have used rapidly multiplexed fields to achieve advanced capabilities. Mode-switching techniques[10] have employed two modes of a standing wave inside a microfluidic channel to position particles across it. The multiplexing of vortices of opposite chirality has removed the transfer of orbital angular momentum and stably trapped larger-than-wavelength particles.[17] Here, we multiplex two different field patterns, a vertical standing wave and a

[a]Electronic mail: luke.cox@bristol.ac.uk

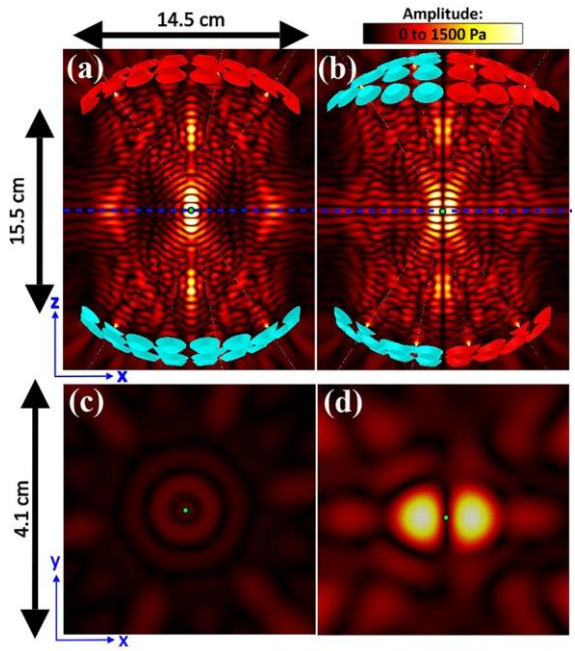

FIG. 1. A 3D Huygens model of the pressure amplitude generated at the two multiplexed states: the standing waves, (a) and (c), and the twin-trap, (b) and (d), seen from the front, (a) and (b), and top, (c) and (d). The green dot indicates the position of the nodes, and the dashed blue line in (a) and (b) indicates the plane of (c) and (d).

twin-trap, to obtain both position and orientation trapping. By changing the amount of time that each field is emitted, we can control the relative forces applied, leading to tunable performance.

The device used in the experiments is made of two opposed spherically capped bowls each consisting of 72 transducers operating at 40 kHz (Manorshi, MSO-A1640H10T, P. R. China) arranged in 4 rings [Fig. 2(a)]. Each bowl can be divided into two symmetric halves [Fig. 2(b)] with an invertible phase to facilitate the emission of both vertical standing waves and twin-traps.

This system requires only four signals to drive the whole array, i.e., one for each half of the two bowls. These signals can be in-phase or out-of-phase with respect to each other, and this allows the device to generate both a vertical standing wave and a twin-trap. This is an advantage compared to

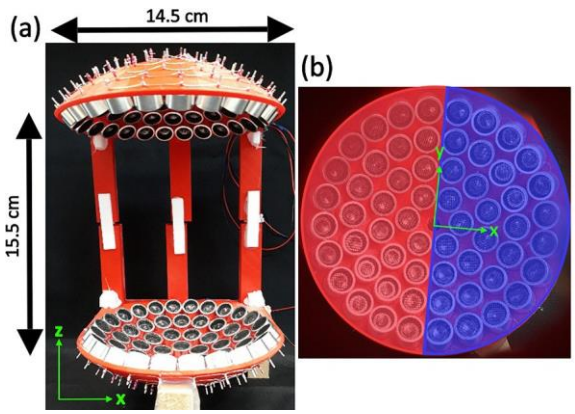

FIG. 2. The acoustic Levitator (a) and one of its spherically capped bowls with the halves overlaid with red and blue (b).

previous devices which require control of each individual channel[16,17] or careful geometric design.[15]

The forces generated by the vertical standing wave and twin-trap, as calculated using the Gor'kov potential approach with the same equipment and transducer output amplitude in all cases, are plotted in Fig. 3. It can be seen in Fig. 3(a) that the vertical standing wave has significantly larger vertical forces than the twin-trap. Figure 3(b) shows that the vertical standing wave also has somewhat larger lateral forces than the twin-trap. However, these forces are symmetrical about the z-axis and thus they cannot generate a converging torque. In contrast, the twin-trap produces large lateral forces in one direction and almost none in the other (F_x F_y). This asymmetric force field produces a converging torque that can lock the orientation of a non-spherical particle.

To model the torque exerted on the particles, we employed a finite-difference time-domain (FDTD) model.[1] Figure 4(a) shows a square particle in a 2D slice in the XY plane of the twin-trap. Two emitters were placed at the sides of the simulation boundary, and the incident pressure amplitude profile was matched to that of a 3D acoustic field simulation (i.e., in the absence of a scatterer) with an R^2 0.9990. The FDTD simulations inherently provide the total field (i.e., incident plus scattered). Using the total field, the force and torque on the particle at different angles can be obtained via evaluation of the momentum flux-integral over the surface of the scatterer[11] (the Gor'kov potential could not be used as it provides no torque information). The torque exerted on a square is shown in Fig. 4(b).

It was found experimentally that a ratio of 100:50 periods (2.5:1.25 ms) of vertical standing wave:twin-trap was the optimal compromise between vertical and horizontal forces for maintaining the stability of 3D-printed plastic and laser cut wooden cuboids. This was applied by 100 periods of the standing wave, followed by 50 periods of the twin-trap. The twin-trap was created by inverting the phase on half of the transducers with no other phase shift or delay. This cycle is then repeated, but the twin-trap created the second time had a phase shift applied to the other half of the bowls. This was necessary as a phase inversion leads to acoustic power loss, so by alternating the side where this occurs, the application of net force is prevented. If the twin-trap emission was too short, samples would spin and ultimately be ejected from the trap. If the twin-trap emission was too long, then the lack of vertical standing wave emission caused position instability

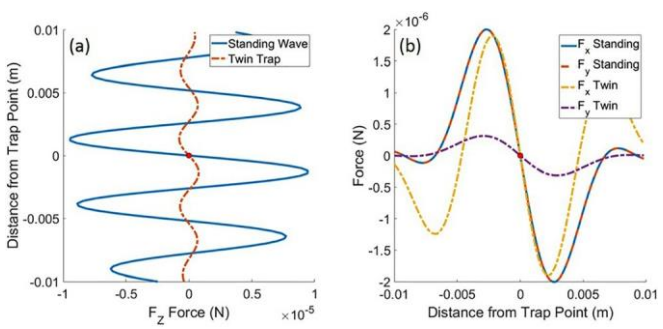

FIG. 3. The forces exerted by the vertical standing wave and twin-trap arrangements in the (a) vertical and (b) horizontal directions. The red dot indicates the central trap point.

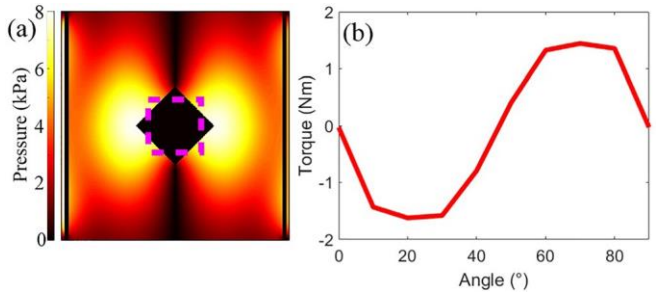

FIG. 4. (a) The total field of the FDTD simulation of a 4 mm side length square at 45° in the horizontal plane of a twin-trap. The pink dashed square represents the 0° rotation position. (b) The torque exerted on the square as predicted by the FDTD model as it rotates about 90°. Note the unstable equilibrium at 45° and the stable ones at 0° and 90°.

in the z-axis with the sample often rocking or even falling out of the trap.

Experiments were conducted to find the range of cube sizes which could be locked in mid-air. A selection of laser-cut wooden cuboids were selected and placed into the trap at a 100:50 ratio. Stable locking was defined as having a net zero location and orientation change once equilibrium was reached combined with location oscillation amplitude of less than 1 mm and a rotational one of less than 10°, as judged by visual inspection. The definition also included resistance to the type of disturbances present in an open laboratory environment, but not deliberate ones generated by physical contact. Figure 5 shows the observed stability of a selection of laser-cut wooden cuboids of different sizes. As the tested objects were both cubes and cuboids, the geometric mean between the sides is plotted.

It can be seen that the stability of the cuboids depends on their side and that qualitatively there is a stable region of sizes. Cubes with sides ranging from $\lambda/5.56$ (1.5 mm) to $\lambda/2.5$ (3.4 mm) were stably locked. The lower limit is due to torque reduction as the particle size decreases, as shown by the blue line. The upper limit is caused by the reduction in acoustic radiation force as the particle size increases, as shown by the orange line.

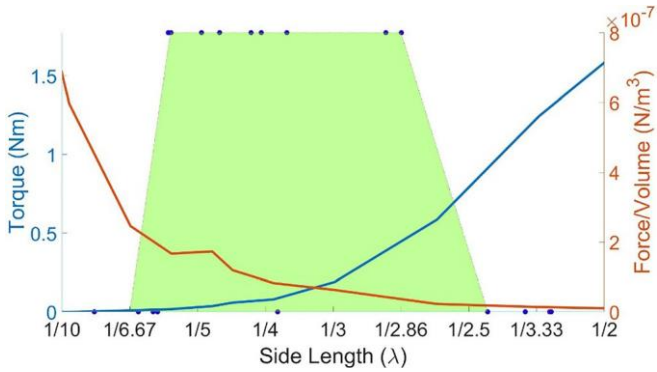

FIG. 5. Stability of cuboids depending on their side length. Each blue dot is a qualitative observation of stability for the average side length of a cuboid. Top points are stable and bottom points are unstable. Instability was due to spinning or inability to levitate. The green region indicates the approximate region of stability based on these experimental results. This region can be qualitatively explained by the intersection between the blue line, representing the exerted torque, and the orange line, representing the radiation force compared to the weight as predicted by the momentum flux integral.

To determine the torsional spring stiffness on the z-axis, we placed an acrylic cuboid (3.2 1.7 1.6 mm, density 1.18 g/cm^3) into the trap with different ratios of the vertical standing wave to the twin-trap. Then, we perturbed one of its corners with a thin metal wire to induce rotational oscillation and recorded the response. A high speed camera (Casio Exilim Ex-ZR100) filmed an ink dot on one side of the block at 240 fps which was tracked by *Tracker Video Analysis and Modelling Tool 4.11.0* (Douglas Brown, 2018). Simple trigonometry approximated the angle of oscillation from the dot position. The time domain oscillations were analysed via Fourier decomposition to calculate the frequency of the rotational oscillation. K_T, the torsional spring constant, was calculated using $K_T = \omega_0^2 I$, where ω_0 is the natural frequency and I the moment of inertia about the vertical axis of the profile of the cuboid from above, calculated by $I = \frac{m}{12}(L_{long}^2 + L_{short}^2)$.

These experimental results were compared with the simulated torsional spring stiffness about the z-axis. The profile of the cuboid was used in the FDTD simulation, and a torque plot similar to Fig. 4(a) was obtained. From the torque plot, the spring stiffness K_T is calculated from the gradient at 0°. This spring stiffness is multiplied by the fraction of time in which the twin-trap is present on the total cycle, i.e., 33.3% for a 100:50 ratio to simulate the multiplexing.

A comparison of experimental and modelled results is shown in Fig. 6. The gradients of the predicted and the experimental line are in good agreement, confirming that the relative strengths of the forces can be "tuned" by the time ratios of their presence. By increasing the ratio of the twin-trap to the vertical standing wave, K_T is increased linearly. However, this decreases the maximum density which can be trapped because it reduces the amount of vertical standing waves emitted. Hence, a compromise must be found depending on the size and density of the object. The employed 100:50 ratio was found to be robust for a reasonable range of sizes of acrylic and wooden cuboids (as illustrated in Fig. 5). Low density samples (such as insects) could be given more lateral stability by increasing the ratio of the twin trap, whilst denser material samples (i.e., larger inertia) could be given more support by increasing the relative amount of vertical standing waves. Practically, this means that the ratio will need to be tuned depending on sample density and there will be an upper limit on density where it is not possible to both lift and stabilise an object. However, a higher density object

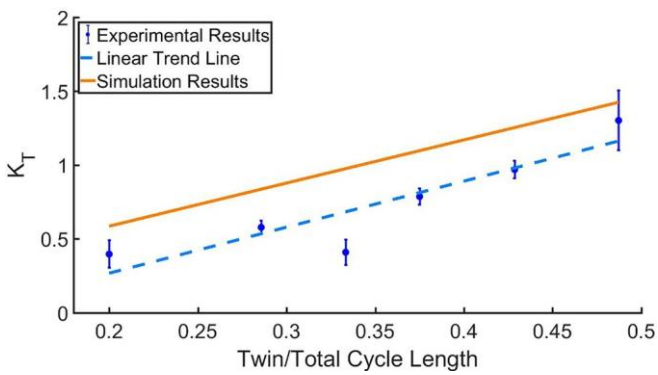

FIG. 6. Experimental and simulated torsional spring stiffness on the z-axis (K_T) for different ratios of vertical standing wave:twin-trap. Error bars represent standard deviation.

will also have more inertia, making it more resistant to any initial disturbances, though once spinning starts, it is unlikely to stabilise due to the larger lateral forces required. The density limit depends on emitter power so is a device specific practical limit, rather than a fundamental one.

Figure 6 shows an offset between the simulated and experimental lines. This is explained by the non-instantaneous switching between the fields leading to some power loss, and the remaining minor inaccuracies are suspected to be due to 2D modelling being applied to a 3D object.

The technique was qualitatively tested on other shapes as shown in Fig. 7, with video proof in the accompanying multimedia view. It was generally found that non-axisymmetric shapes could be reliably locked. Figure 7(b) shows that some axisymmetric objects could be locked but others, such as a cones or toroids, could not and instead tended to rotate about their axis of symmetry.

Other asymmetric samples such as insects can be locked with our technique. The possibility of trapping insects in both the position and the orientation represents a significant improvement over previous levitators for analysing levitated living things.[21,24] Although the focus of this paper was on solid cuboids at room temperature, some brief trials of other shapes, liquids, and heating were also conducted, with details provided in the supplementary material.

We have presented a technique for stable 3D trapping in the position and orientation of non-spherical sub-wavelength objects using acoustic levitation. A converging torque has been shown by measuring the torsional spring factor, and the technique has been demonstrated using a variety of objects locked in mid-air. The acoustic trapping of non-spherical objects has usually been neglected in the literature despite being an important problem faced by practical applications of acoustic levitation.

See supplementary material for full specifications of the device. It also gives further details on the 3D Huygens and the FDTD models. It details the momentum-flux integral used for the forces and torque. It shows the matching between the incidental 3D Huygens model field and the FDTD model for torque calculations. It shows a larger regime of the torque vs particle size length relationship. It explains in detail the power loss offset of the simulated and experimental K_T lines and details further experiments conducted on liquids and heated samples. The video demonstrates the working of the acoustic lock in more detail.

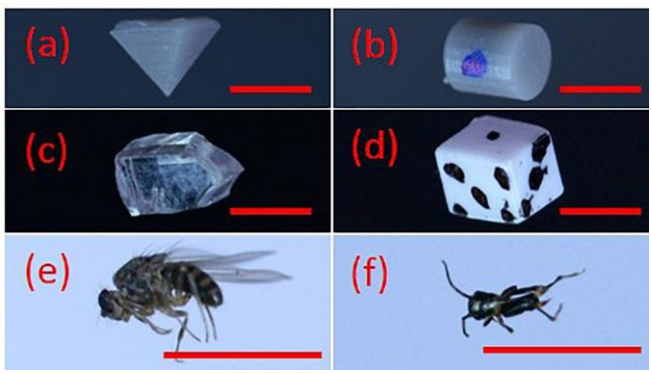

FIG. 7. Acoustic locking of various non-spherical objects: (a) a pyramid, (b) a cylinder (with a dot on the side to confirm it was not rotating), (c) a piece of acrylic, (d) a small dice, (e) a fruit fly (exposure time ¼ 1/1250 s), and (f) a micro-cricket (exposure time ¼ 1/2500 s). Images are taken with a Nikon D610 camera equipped with a Sigma 105 f2.8 lens. The scale bar is 3 mm. Multimedia view: https://doi.org/10.1063/1.5042518.1

This project was funded by the UK Engineering and Physical Science Research Council (No. EP/N014197/1). L.C. was funded by a CASE studentship in collaboration with Ultrahaptics. Sufficient information is available within this paper and supplementary material to recreate these results. The data presented in this work are openly available at Zenodo https://doi.org/10.5281/zenodo.1319571.

[1]A. Allen and N. Raghuvanshi, "Aerophones in flatland: Interactive wave simulation of wind instruments," ACM Trans. Graphics (TOG) 34(4), 134 (2015).
[2]M. A. B. Andrade, T. S. Ramos, F. T. A. Okina, and J. C. Adamowski, "Nonlinear characterization of a single-axis acoustic levitator," Rev. Sci. Instrum. 85(4), 045125 (2014).
[3]S. Baer, M. A. B. Andrade, C. Esen, J. C. Adamowski, and A. Ostendorf, "Development of a single-axis ultrasonic levitator and the study of the radial particle oscillations," AIP Conf. Proc. 1433, 35–38 (2012).
[4]M. V. Berry and A. K. Geim, "Of flying frogs and levitrons," Eur. J. Phys. 18(4), 307 (1997).
[5]E. H. Brandt, "Acoustic physics: Suspended by sound," Nature 413(6855), 474 (2001).
[6]H. Bruus, "Acoustofluidics 7: The acoustic radiation force on small particles," Lab Chip 12(6), 1014–1021 (2012).
[7]A. El Hajjaji and M. Ouladsine, "Modeling and nonlinear control of magnetic levitation systems," IEEE Trans. Ind. Electron. 48(4), 831–838 (2001).
[8]D. Foresti, M. Nabavi, M. Klingauf, A. Ferrari, and D. Poulikakos, "Acoustophoretic contactless transport and handling of matter in air," Proc. Natl. Acad. Sci. 110(31), 12549–12554 (2013).
[9]A. K. Geim, M. D. Simon, M. I. Boamfa, and L. O. Heflinger, "Magnet levitation at your fingertips," Nature 400(6742), 323 (1999).
[10]P. Glynne-Jones, R. J. Boltryk, N. R. Harris, A. W. J. Cranny, and M. Hill, "Mode-switching: A new technique for electronically varying the agglomeration position in an acoustic particle manipulator," Ultrasonics 50(1), 68–75 (2010).
[11]R. Habibi, C. Devendran, and A. Neild, "Trapping and patterning of large particles and cells in a 1d ultrasonic standing wave," Lab Chip 17(19), 3279–3290 (2017).
[12]L. V. King, "On the acoustic radiation pressure on spheres," Proc. R. Soc. London A 147(861), 212–240 (1934).
[13]E. J. Kramer, "Scaling laws for flux pinning in hard superconductors," J. Appl. Phys. 44(3), 1360–1370 (1973).
[14]A. Marzo, A. Barnes, and B. W. Drinkwater, "Tinylev: A multi-emitter single-axis acoustic levitator," Rev. Sci. Instrum. 88(8), 085105 (2017).
[15]A. Marzo, A. Ghobrial, L. Cox, M. Caleap, A. Croxford, and B. W. Drinkwater, "Realization of compact tractor beams using acoustic delay-lines," Appl. Phys. Lett. 110(1), 014102 (2017).
[16]A. Marzo, S. A. Seah, B. W. Drinkwater, D. R. Sahoo, B. Long, and S. Subramanian, "Holographic acoustic elements for manipulation of levitated objects," Nat. Commun. 6, 8661 (2015).
[17]A. Marzo, M. Caleap, and B. W. Drinkwater, "Acoustic virtual vortices with tunable orbital angular momentum for trapping of MIE particles," Phys. Rev. Lett. 120(4), 044301 (2018).
[18]N. A. Mauro and K. F. Kelton, "A highly modular beamline electrostatic levitation facility, optimized for in situ high-energy x-ray scattering studies of equilibrium and supercooled liquids," Rev. Sci. Instrum. 82(3), 035114 (2011).
[19]A. O. Santillán, K. Volke-Sepúlveda, and R. R. Boullosa, *Acoustically Controlled Rotations of a Disk in Free Field* (International Institute of Acoustics and Vibration, 2007).
[20]T. Schwarz, P. Hahn, G. Petit-Pierre, and J. Dual, "Rotation of fibers and other non-spherical particles by the acoustic radiation torque," Microfluid. Nanofluid. 18(1), 65–79 (2015).
[21]H. J. Sundvik, M. Nieminen, A. Salmi, P. Panula, and E. Hæggström, "Effects of acoustic levitation on the development of zebrafish, Danio rerio, embryos," Sci. Rep. 5, 13596 (2015).

[22]V. Vandaele, A. Delchambre, and P. Lambert, "Acoustic wave levitation: Handling of components," J. Appl. Phys. 109(12), 124901 (2011).
[23]R. R. Whymark, "Acoustic field positioning for containerless processing," Ultrasonics 13(6), 251–261 (1975).
[24]W. J. Xie, C. D. Cao, Y. J. Lü, Z. Y. Hong, and B. Wei, "Acoustic method for levitation of small living animals," Appl. Phys. Lett. 89(21), 214102 (2006).
[25]Q. Xiu-Pei, G. De-Lu, H. Zhen-Yu, and W. Bing-Bo, "Rotation mechanism of ultrasonically levitated cylinders," Acta Phys. Sin. 66(12), 124301 (2017).
[26]A. L. Yarin, G. Brenn, J. Keller, M. Pfaffenlehner, E. Ryssel, and C. Tropea, "Flowfield characteristics of an aerodynamic acoustic levitator," Phys. Fluids 9(11), 3300–3314 (1997).